Journal of Magnetic Resonance **141,** 207–216 (1999)
Article ID jmre.1999.1902, available online at http://www.idealibrary.com on IDEAL®

Quantification of Regional Intrapulmonary Oxygen Partial Pressure Evolution during Apnea by ^{3}He MRI

A. J. Deninger,*[,1] B. Eberle,† M. Ebert,* T. Großmann,* W. Heil,* H.-U. Kauczor,‡ L. Lauer,* K. Markstaller,‡ E. Otten,* J. Schmiedeskamp,* W. Schreiber,‡ R. Surkau,* M. Thelen,‡ and N. Weiler†

*Department of Physics, †Department of Anesthesiology, and ‡Department of Radiology, University of Mainz, D-55099 Mainz, Germany

Received January 19, 1999; revised July 29, 1999

We present a new method to determine *in vivo* the temporal evolution of intrapulmonary oxygen concentrations by functional lung imaging with hyperpolarized ^{3}Helium ($^3\overrightarrow{\text{He}}$). Single-breath, single-bolus visualization of $^3\overrightarrow{\text{He}}$ administered to the airspaces is used to analyze nuclear spin relaxation caused by the local oxygen partial pressure $p_{O_2}(t)$. We model the dynamics of hyperpolarization in the lung by rate equations. Based hereupon, a double acquisition technique is presented to separate depolarization by RF pulses and oxygen induced relaxation. It permits the determination of p_{O_2} with a high accuracy of up to 3% with simultaneous flip angle calibration using no additional input parameters. The time course of p_{O_2} during short periods of breathholding is found to be linear in a pig as well as in a human volunteer. We also measured the wall relaxation time in the lung and deduced a lower limit of 4.3 min. © 1999 Academic Press

Key Words: **hyperpolarized gas MRI; functional imaging; MRI of lung; intrapulmonary oxygen; oxygen concentration.**

1. INTRODUCTION

The recent success of hyperpolarized gas imaging has stimulated considerable interest in medical applications, especially in lung studies. Since 1994, several groups have demonstrated the feasibility of magnetic resonance imaging (MRI) of ventilated air spaces in animals and humans using nuclear spin polarized ^{3}Helium ($^3\overrightarrow{\text{He}}$) (*1–7*) or ^{129}Xenon (*8–11*). First clinical studies by Kauczor *et al.* (*12, 13*) have shown the diagnostic potential of $^3\overrightarrow{\text{He}}$ imaging for lung diseases. In all these examinations, optical pumping of nuclear spins 1/2 serves to achieve a polarization level up to five orders of magnitude higher than equilibrium (Boltzmann) polarization. Here and in the following, polarization P is defined by

$$P = \frac{N^+ - N^-}{N^+ + N^-}, \qquad [1]$$

where N^+ (N^-) denotes the number of spins parallel (antiparallel) to the external magnetic field B_0.

[1] This publication contains part of the Ph.D. thesis of A. J. Deninger.

In the beginning of $^3\overrightarrow{\text{He}}$ MRI, molecular oxygen has been considered as an obstacle, as dipolar coupling between nuclear spins of ^{3}He and electronic spins of paramagnetic O_2 leads to rapid longitudinal relaxation (*14*) and hence irreversible loss of hyperpolarization. In some experiments, the effect was reduced by flushing the lungs with ^{4}He prior to imaging [e.g., (*3, 7, 12*)]. In this study, we pursue a contrary approach: the decay of polarization in subsequent images acquired during breathholding (inspiratory apnea) is used to determine relaxation rates which, in turn, enable precise quantification of the oxygen partial pressure and its temporal evolution in the respective volumes.

In a first publication on this topic (*15*), we reported about an experiment where global pulmonary oxygen concentrations, as detected by MRI, were compared with end-expiratory values. Statistical data from six pigs showed a strong correlation of 87.9% between results. Basing on this experience, we present in this work a procedure which allows simultaneous determination of both the local, time-dependent oxygen partial pressure and the local flip angle of MR excitations. An accuracy of p_{O_2} of up to 3% has been reached. An MR image based analysis of p_{O_2} within a silicon bag was carried out to verify our theory. The agreement with the preadjusted oxygen concentration was very good. Further experiments were performed in two pigs and one human volunteer. Imaging of a dead pig's lung also enabled to assess an upper limit of wall relaxation by lung tissue in the absence of oxygen.

2. THEORY

Consider a ventilated area of the lung imaged by MRI. Irreversible loss of the high nonequilibrium polarization P of inhaled $^3\overrightarrow{\text{He}}$ inside this volume is caused by three mechanisms. These are NMR excitations, relaxation due to the presence of molecular oxygen and wall relaxation by lung tissue. Further relaxation sources, namely by ^{3}He–^{3}He dipolar coupling (*16*) and by magnetic field gradients (*17, 18*) may be neglected under the present conditions. The three relevant effects will now be discussed separately, leading to a system of two cou-

1090-7807/99 $30.00
Copyright © 1999 by Academic Press
All rights of reproduction in any form reserved.

pled differential equations modeling the dynamics of the polarization.

Let α be the flip angle of the magnetization by a single RF pulse. If an image is acquired using a sequence consisting of N RF pulses separated by a repetition time T_R, these excitations result in an apparent relaxation rate Γ_{RF} given by

$$\Gamma_{RF}(t) = -\ln(\cos\alpha)/T_R, \qquad [2]$$

while sampling k-space.

Relaxation of $^3\overrightarrow{He}$ by O_2 is studied in (*14*), where the following rate was found (recalculated for body temperature)

$$\Gamma_{O_2} = 0.38 \cdot p_{O_2}\text{bar}^{-1}\text{s}^{-1} = \frac{p_{O_2}}{\xi}, \qquad [3]$$

with p_{O_2} being the oxygen partial pressure (in bar) and the coefficient $\xi = 2.61$ bar $\cdot$ s.

The wall relaxation rate Γ_w depends on the surface to volume ratio S/V of the structure enclosing the gas and can hence be described by

$$\Gamma_w = \frac{1}{\eta}\frac{S}{V}, \qquad [4]$$

where η is a specific relaxation coefficient of the wall material.

In addition to the relaxation rates [2] to [4], $^3\overrightarrow{He}$ exchange with the nonexcited surroundings affects the polarization $P(t)$ inside an imaged slice. Let $P'(t)$ be the polarization in these nonimaged volumes, which decreases only due to oxygen and wall relaxation. In a simplifying "two compartment model" one then obtains two rate equations describing the temporal evolution of P and P', which are coupled by a term $(P - P')$ driving the mutual gas exchange, e.g., by diffusion. Introducing two characteristic coefficients γ and γ', these equations read

$$\dot{P} = -\Gamma_{O_2}(t)\,P - \Gamma_{RF}(t)\,P - \Gamma_w P + \gamma(P' - P) \qquad [5]$$

$$\dot{P}' = -\Gamma_{O_2}(t)\,P' - \Gamma_w P' - \gamma'(P' - P). \qquad [6]$$

Here we have assumed that within the lung tissue, Γ_{O_2} and Γ_w do not vary significantly on the scale of a typical diffusion length acquired during the time of measurement. Boundary regions have to be treated differently and are not considered here. Furthermore, we take the initial polarization $P_0 \equiv P(t = 0)$ to be the same in the entire lung.

We will present analytical solutions for two different experimental conditions. These are:

(a) All spins in the lung are equally excited. This greatly simplifies matters and is to be preferred in practical applications. In this case, the effect of gas exchange is rendered unobservable, i.e., $(P - P') \approx 0$ for all times. Experimentally, it can be achieved either by use of thick slices in 2D techniques, or by 3D acquisitions covering the entire inhaled volume of $^3\overrightarrow{He}$.

(b) The volume V of the imaged partition is thin compared to the surrounding volume V' with which diffusive contact exists within the time scale of a typical imaging sequence. In this case γ and γ' scale according to the ratio of the volumes involved, hence $\gamma' = \gamma \cdot V/V'$. Thus γ' may be neglected if $V \ll V'$.

The solutions of [5] and [6] will now be discussed separately for the two cases specified above.

In case (a) the rate equation [5] is easily integrated. For analysis of $P(t)$ we assume that images be taken at fixed times t_n $(n = 0, 1, 2 \ldots, \nu)$. These are, for instance, the sampling times of central k-space lines $k = 0$, which yield the main contrast in each image. Denoting the signal intensities of pictures taken at times t_n by A_n, a solution of [5] is given by

$$A_n = A_0(\cos\alpha)^{nN} e^{-\Gamma_w t_n} e^{-\int_0^{t_n}\Gamma_{O_2}(t)dt}. \qquad [7]$$

In case (b), we first solve Eq. [6] under the condition $\gamma' = 0$ and insert the solution for P' into Eq. [5]. For convenience, we also introduce a time averaged RF relaxation rate

$$\bar{\Gamma}_{RF} = -\nu N \ln(\cos\alpha)/T_{tot} \qquad [8]$$

(ν index number of last image, $T_{tot} = t_\nu$ duration of measurement) which substitutes for the nonsteady time course of $\Gamma_{RF}(t)$. Thereby the solution of [5] yields for the signal intensities

$$A_n = \frac{A_0}{\gamma + \bar{\Gamma}_{RF}}\{\bar{\Gamma}_{RF}(\cos\alpha)^{nN} e^{-(\Gamma_w+\gamma)t_n} \times e^{-\int_0^{t_n}\Gamma_{O_2}(t)dt} + \gamma e^{-\Gamma_w t_n} e^{-\int_0^{t_n}\Gamma_{O_2}(t)dt}\}. \qquad [9]$$

For $\gamma \to 0$ (which is equivalent to the thick partition limit), [9] reduces to [7]. In general, Eq. [9] provides a basis to determine gas movements within the lung from changes in image intensities. A qualitative confirmation has been observed experimentally. However, as results are still subject to further investigation and do not fall within the scope of this publication, they are not discussed any further.

For data analysis, it is simpler to work with logarithmic signal intensities E_n, normalized to the initial intensity A_0, averaged over a given region of interest (ROI):

$$E_n \equiv \ln\left(\frac{A_n}{A_0}\right). \qquad [10]$$

Disregarding wall relaxation, which will be justified by exper-

iments described in Section 4.1, the E_n still depend on both α and Γ_{O_2}. In order to determine both effects separately, the parameter Γ_{RF} which is accessible to the MR operator has to be varied between images, so that MR induced relaxation is discriminated from oxygen relaxation (Γ_{O_2}). In our experiments, a double acquisition technique proved successful: two series of images are taken, while either the RF amplitude or the interscan time $\tau = (t_{n+1} - t_n)$ was changed between series. The idea is best illustrated by a simple example. Consider a set of images with a single thick slice (i.e., suppressing diffusion effects). If images are taken in equidistant interscan times (hence, $t_n = n \cdot \tau$), Eq. [7] can be rewritten

$$E_n = Nn \ln(\cos \alpha) - \int_0^{n\tau} \Gamma_{O_2}(t)dt. \qquad [11]$$

Method 1

The second set of images is acquired retaining τ, but multiplying α by a factor of κ. Assuming p_{O_2} and its time development to be equal in a given ROI during both series, the E_n values of corresponding images can be subtracted giving

$$\frac{E_n(\alpha) - E_n(\kappa\alpha)}{N} = n \ln\left(\frac{\cos \alpha}{\cos \kappa\alpha}\right). \qquad [12]$$

If the left-hand side of [12] is plotted against n, ln (cos α/cos $\kappa\alpha$) and furtheron α are obtained from the slope. In a second step, Eq. [11] of either dataset is corrected for flip angle effects, and Γ_{O_2} is extracted by a fit.

Method 2

The second set of images is acquired with the same RF amplitude, but with a different τ. In this case, subtraction of corresponding E_n values results in elimination of the (cos α) term in Eq. [11]:

$$\xi \cdot (E_n(\tau_1) - E_n(\tau_2)) = \int_0^{n\tau_2} p_{O_2}(t)dt - \int_0^{n\tau_1} p_{O_2}(t)dt. \qquad [13]$$

Thus, information about the temporal development of p_{O_2} is obtained. By correcting Eq. [11] for this relaxation effect, depolarization by RF excitations can be computed.

3. METHOD AND MATERIALS

3.1. Production and Administration of $^3\overrightarrow{He}$

The technical details of production and supply of $^3\overrightarrow{He}$ at the University of Mainz have been reported elsewhere (*19–22*). Briefly summarized, hyperpolarization is achieved by direct optical pumping from the metastable $1s2s^3S_1$ state at 1 mbar pressure, using a Krypton arc-lamp pumped LNA ($La_{0.85}Nd_{0.15}MgAl_{11}O_{13}$) solid state laser. A two-stage titanium piston compressor accomplishes compression to convenient pressures of 1 to 6 bar preserving polarization. The apparatus described in (*22*) reaches nuclear spin polarizations of up to 50% at a flow of 3.5×10^{18} atoms/s and still 40% at 8×10^{18} atoms/s. The gas is filled into glass cells (volume 360 . . . 500 ml, pressure typically 3 bar). For experiments reported upon here, uncoated cells made of low iron content Supremax glass (Schott Glaswerke, Mainz, Germany) with relaxation times of 20 to 70 h were used. They can be closed by a stop cock and disconnected from the filling system. For transport to the MR imaging unit at the Department of Radiology, cells are stored inside a shielded 0.3 mT guiding field. Inside the MR scanner, the $^3\overrightarrow{He}$ samples are connected to a gas administration unit designed and built by our group. The device permits administration of $^3\overrightarrow{He}$ boli of fixed volume (20 . . . 500 ml at atmospheric pressure) into the inspiratory tidal volume at any predefined time, with high accuracy ($\pm$5 ml) and negligible loss of hyperpolarization. Its principle is as follows. $^3\overrightarrow{He}$ is allowed to expand into a flexible bag positioned within a rigid cylinder, which can be pressurized to expel the gas via a switch valve out of the bag and into a short tube leading to the mouth of the imaged subject. The entire gas administration unit is controlled by a PC. While the administration unit is placed within the homogeneous field inside the scanner, the PC control unit is set up in an adjacent room. Volunteers or patients can either breathe spontaneously through the application unit, or ventilation can be supported by a commercial respirator unit.

3.2. Study Objects

3.2.1. Phantom experiment. In order to test the prediction of the theory outlined in Section 2, an *in vitro* experiment was performed imaging $^3\overrightarrow{He}$ in a silicon bag. The volume of the bag was 560 ml including deadspace from tubings. The bag was connected to a respirator unit (Servo 900 C, Siemens-Elema, Erlangen, Germany) and ventilated with O_2-enriched air (oxygen concentration 22%). The respirator operated at an excess pressure of $\approx$20 mbar. A wooden board was put onto the bag to squeeze out the air during "exhalation." A previous measurement of wall relaxation in a similar bag had established a wall relaxation time of $\mathbb{C}$(40 min), hence wall relaxation effects could be neglected in the imaging experiment.

3.2.2. Animal model. With animal care committee approval, two pigs (28 $\pm$ 1 kg) underwent volume controlled ventilation (15 breaths per minute, tidal volume 580 $\pm$ 13 cm^3, inspiratory oxygen concentration 21%). Anesthesia was maintained by intravenous administration of piritramide (1.2 mg kg^{-1}) and thiopental (15 mg kg^{-1} h^{-1}). Intraarterial and intravenous femoral catheters served for pressure monitoring and drug administration. After stabilization, the animals were transferred into the MR scanner and positioned supine. $^3\overrightarrow{He}$ was given by the application unit via an endotracheal tube. Wall

relaxation in the lung was measured after cardiac arrest had been induced by KCl injection under anesthesia (see Section 4.1).

3.2.3. Human subject. A healthy male volunteer (age 24 years, weight 72 kg) was placed inside the scanner in supine position. The gas applicator was used to administer $^3\overrightarrow{He}$ via a mouth piece during spontaneous breathing. During imaging, breathholds were maintained with the nose clamped.

Images were acquired during inspiratory apnea. After initial inspiration of 60 ml of the inspiratory O_2/N_2 mixture from dead volumes of gas applicator tubings, a bolus of $^3\overrightarrow{He}$ was administered, followed by a second O_2/N_2 bolus. Bolus volumes were 80 cm^3 $^3\overrightarrow{He}$ + (400 ± 13) cm^3 O_2/N_2 in the phantom experiment, 100 cm^3 $^3\overrightarrow{He}$ + (420 ± 13) cm^3 O_2/N_2 in the animal model, and 180 cm^3 $^3\overrightarrow{He}$ + (610 ± 40) cm^3 O_2/N_2 in the human volunteer. End-expiratory oxygen concentrations were not monitored in this study. The phantom experiment demonstrated excellent agreement between the adjusted oxygen concentration and MR-determined results.

3.3. MR Image Acquisition

Measurements were performed within a conventional whole body scanner at $B_0 = 1.5$ T (Magnetom Vision, Siemens Medical Systems, Erlangen, Germany). MR transitions and signals were transmitted by a dedicated custom-built coil (Fraunhofer Institut, St. Ingbert, Germany) which was a dual ring construction with a sensitive volume of 365 × 340 × 450 mm^3 (L × W × H), double resonant on the ^{3}He Larmor frequency at 48.44 MHz as well as on that of ^{1}H at 63.86 MHz. A 2D FLASH gradient echo sequence was used with repetition time $T_R = 11$ ms, echo time $T_E = 4.2$ ms, field of view (320 mm)^2, acquisition matrix 81 × 128, image acquisition time 0.9 s. The *k*-space was sampled in a centric reordering fashion. RF excitation amplitudes were 5, 10, or 20 Volts, time intervals τ between images ranged from 1 to 7 s. Thick partitions in coronal orientation (120 mm in phantom and pigs, 180 mm in the human lung) were utilized.

3.4. Data Analysis

Images were analyzed on a PC using standard software (program NMRWin medical imaging system, version 3.33, German Cancer Research Center, Heidelberg, Germany). In a preselected ROI within the image, the distribution of pixel intensities as well as the mean intensity were computed with 12-bit resolution. Chosen ROIs typically comprised 50 to 450 pixel, corresponding to an area of 0.8 to 7 cm^2. Obviously, a mean intensity is meaningful only if the intensity distribution in the ROI is sufficiently homogenous and does not contain, for instance, major blood vessels, or large airways out of which $^3\overrightarrow{He}$ has been driven into the alveoles by the second O_2/N_2 bolus.

The mean intensities M were then corrected for the noise σ, which introduces a bias in the Fourier transformed quantity M.

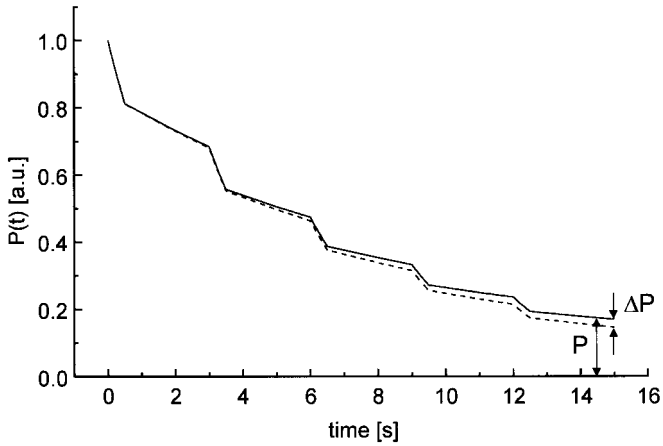

FIG. 1. Simulation of the decay of ^{3}He polarization $P(t)$ in the lung during imaging. The broken line refers to a constant oxygen partial pressure of 0.185 bar, corresponding to inhalation of room air into a pig's functional residual capacity (FRC). The full line depicts the case of an oxygen partial pressure decreasing at a rate of $R = 0.0035$ bar/s. The steep slopes occur due to oxygen relaxation plus RF excitations during image taking, the shallow ones solely due to oxygen relaxation between images.

Since signal to noise ratios were always larger than 3, a bias corrected intensity A_{corr} can be obtained via the approximate formula (*23, 24*)

$$A_{corr} = \sqrt{M^2 - \frac{2}{\pi}\sigma^2}. \qquad [14]$$

This requires but a simple postprocessing of data.

Previous experiments, in which a glass cell filled with $^3\overrightarrow{He}$ was imaged, had established an approximate empirical relation between the variation ΔM of M and pixel number L of a ROI

$$\Delta M \propto \sigma L^{-0.45}, \qquad [15]$$

which is slightly weaker than the usual $L^{-1/2}$ law. Equation [15] is used to compute error bars in the following examples.

The experiment aims not only at the determination of the mean oxygen concentration in a particular ROI but also of its precise change during apnea. The demands on signal-to-noise ratio (SNR) and data analysis are thus unusually high. This is illustrated in Fig. 1, where we have simulated the time evolution of ^{3}He polarization inside the lung during a typical imaging sequence, both for a time-constant oxygen partial pressure and one decreasing at a typical rate. The relative difference $\Delta P/P$ between both polarization decays develops slowly in time but attains no more than 14% (relative) for the last image taken 15 s after inspiration.

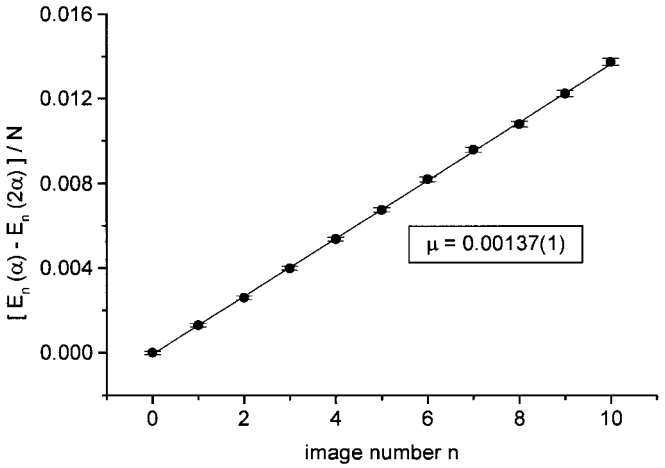

FIG. 2. Determination of flip angle α from subtracted logarithmic intensities E_n. The slope μ of the graph is equal to ln(cos α/cos 2α).

4. RESULTS

Single-breath, single-bolus imaging of $^3\overrightarrow{He}$ was achieved with good SNR (6 . . . 90). Different oxygen concentrations, their temporal evolution as well as corresponding flip angles could be quantified simultaneously from magnitude image analysis. In this section, results of image analysis will be presented with typical examples.

4.1. Determination of Intrapulmonary Wall Relaxation

In a first, exploratory experiment the effect of wall relaxation Γ_w was searched for in a deoxygenized lung of a dead pig by double acquisition sampling with varied flip angles (method 1 in Section 2). Immediately after inducing cardiac arrest, oxygen was washed out by ventilating with pure nitrogen for about 15 min. Subsequently, two series of 11 images each were taken, with RF amplitudes $U_{RF} = 10$ V in the first and $U_{RF} = 5$ V in the second series. Partition thickness was 120 mm in coronal orientation in order to excite $^3\overrightarrow{He}$ spins in the entire lung volume. Interscan time τ was 7 s. ROIs within different parts of the lung were examined. Figure 2 refers to a ROI of 415 pixel (6.5 cm^2) within the cranial right lung. Shown is the difference of logarithmic intensities (Eq. [12]), plotted against image number n. The slope $\mu = \ln[(\cos \alpha)/(\cos 2\alpha)]$ is extracted by a linear fit with a χ^2 per degree of freedom (p.d.f.) of 0.42, giving $\mu = 0.00137(1)$. From this the flip angle for 5 V excitation is found to be $\alpha = 1.73(1)°$. The value varies significantly across the total image: in the caudal right lung, $\alpha = 1.78(1)°$ was measured; in the caudal left lung, the value was $\alpha = 1.97(1)°$. The discrepancy is attributed to inhomogenieties in the response of the transmit/receive coil and RF losses; i.e., the RF amplitude is not constant over the imaged volume. This effect necessitates local flip angle calibration for accurate functional imaging.

Figure 3 depicts the intensities $B_n(t_n) = A_n(t_n)(\cos \alpha)^{-nN}$ after correction for flip angle depolarization. A time constant of longitudinal relaxation $T_1 = 261(4)$ s is fitted to the data with a χ^2 of 1.11 p.d.f. The uncertainty of $\Delta\alpha$ gives rise to a systematic error of ± 2.5 s. The result deserves a few remarks. The value is consistent with another one measured in a dead guinea pig (*1*) where "observable signal" is reported to have been found after 3.5 min. However, some residual oxygen might still contribute to relaxation. An actual oxygen partial pressure of only 9 mbar would suffice to produce the measured relaxation time, an amount we consider possible. In other parts of the lung, relaxation times of 246(6) s (caudal right lung) and 242(4) s (caudal left lung) were measured, which may be taken as a hint toward slightly higher residual oxygen concentrations. Hence, our value of 261 s should be understood as a lower limit of an intrapulmonary wall relaxation time

$$T_{1w} = \Gamma_w^{-1} > 261 \text{ s}. \qquad [16]$$

Even this lower limit, though, yields a remarkably large specific relaxation time coefficient (Eq. [4]) of $\eta > 22$ h/cm, assuming spherical alveoles with an average diameter of 200 μm. The value of η is larger than that of most bare glass surfaces and a number of metallic coatings (*21*). Taken at face value, it means that nondiseased broncho-alveolar surfaces are virtually devoid of radicals or other depolarizing paramagnetic centers. For our case, wall relaxation turns out to be a negligible effect and is omitted in further analysis from now.

4.2. In Vitro Measurement of p_{O_2}

Imaging of a silicon bag ventilated with a preselected oxygen concentration served to test the reliability of our MR-based oxygen measurement. Considering the adjusted oxygen admixture, given bolus volumes and the excess pressure of the

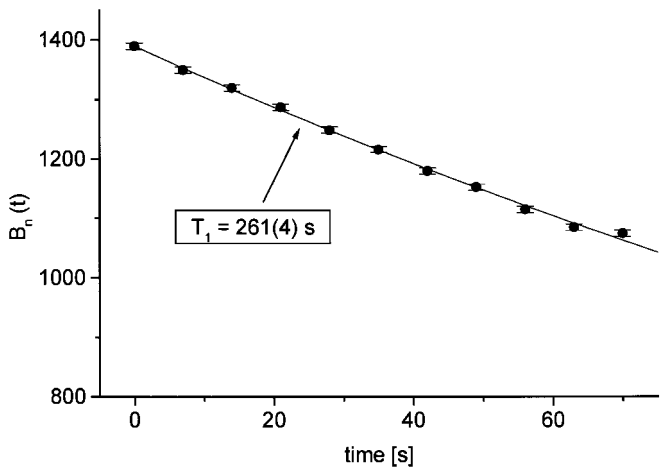

FIG. 3. Measurement of wall relaxation. Intensities $B_n(t_n)$ at times $t_n = n \cdot \tau$, $\tau = 7$ s are corrected for flip angle depolarization. $T_1 = 261(4)$ s is fitted from the monoexponential decay.

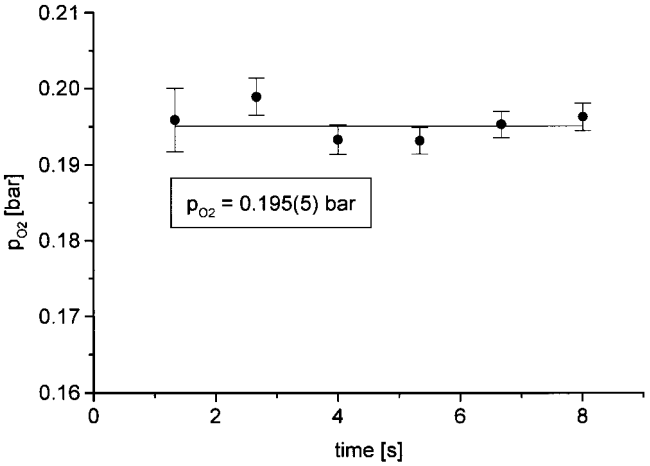

FIG. 4. Measurement of oxygen partial pressure p_{O_2} in a silicon bag. Logarithmic intensities, corrected for flip angle depolarization, are rescaled to give p_{O_2}.

respirator unit as listed in Section 3, one calculates a value of the oxygen partial pressure of $p_{O_2} = 0.193$ bar.

Like in Section 4.1, imaging was performed with different RF amplitudes (method 1). However, to minimize any systematic errors resulting from variations in gas composition, only one imaging sequence was run: 7 images with $U_{RF} = 5$ V were taken, followed immediately by 6 images with $U_{RF} = 20$ V. Partition thickness was 120 mm in coronal orientation, interscan time was $\tau = 2.67$ s. The analysis was carried out as described in the previous example. Within a ROI of 405 pixel (6.3 cm^2), a flip angle of 1.08(2)° for 5 V excitation was computed. Since the gas admixture does not change during the time of measurement, it is reasonable to postulate that $p_{O_2} = const$. Thus Eq. [7] can be rearranged to yield

$$p_{O_2} = \frac{\xi}{t_n}\{nN \ln(\cos \alpha) - E_n\}. \quad [17]$$

Considering the temperature dependence of ξ according to (*14*), a value of $\xi = 2.40$ bar · s, corresponding to room temperature, must be used here. The result of the measurement is shown in Fig. 4, where the right-hand side of Eq. [17] is plotted versus time. The assumption of a constant oxygen partial pressure is confirmed: the slope of a linear fit is zero within errors. Taking into account systematic errors due to flip angle calculation and the 2% intrinsic uncertainty of ξ (*14*), we obtain a mean value of $p_{O_2} = 0.195(5)$ bar with a χ^2 of 1.27 p.d.f. This value is in excellent agreement with the preset value, validating this means of oxygen determination.

4.3. In Vivo Measurement of p_{O_2} in the Porcine Lung

In this section, we present an example of *in vivo* oxygen determination, as obtained from double acquisition sampling with varied interscan time τ (method 2). An anesthetized pig underwent controlled ventilation with room air (oxygen concentration 21%). After $^3\overrightarrow{He}$ bolus injection, a series of 8 images with $\tau_1 = 7$ s was acquired during inspiratory apnea (≈50 s). After a short interval to ensure stability of vital parameters, a second series of 8 images with $\tau_2 = 1$ s was taken. RF amplitude was 10 V in both series, partition thickness was 120 mm in coronal orientation.

The oxygen partial pressure $p_{O_2}(t)$ is determined from the sequence of normalized logarithmic intensities $E_1, E_2 \ldots E_n$ via Eq. [13]. The procedure is simplified if we assume a priori that the time dependence of p_{O_2} be linear

$$p_{O_2}(t) = p_0 - Rt, \quad [18]$$

where R is the rate of oxygen decrease. This is certainly a reasonable first-order approximation which has also been confirmed in another control animal by measurements of end-expiratory $p_{O_2}(t)$ after periods of inspiratory apnea for times up to 35 s. There a rate of $R \approx 0.002$ bar/s was found.

Equation [13] can then be integrated giving

$$\xi \cdot (E_n(\tau_1) - E_n(\tau_2)) = np_0(\tau_2 - \tau_1) - \frac{R}{2} n^2(\tau_2 - \tau_1)(\tau_2 + \tau_1). \quad [19]$$

Division by $n(\tau_2 - \tau_1)$ yields

$$y_n = \xi \frac{E_n(\tau_1) - E_n(\tau_2)}{n(\tau_2 - \tau_1)} = p_0 - R\left(\frac{n}{2}(\tau_1 + \tau_2)\right). \quad [20]$$

Comparison with Eq. [18] shows that the experimental quantities y_n just equal the searched for oxygen partial pressure

$$y_n = p_{O_2}(\bar{t}_n) \quad [21]$$

at mean times $\bar{t}_n = n(\tau_1 + \tau_2)/2$.

In Fig. 5 we have plotted the course of $p_{O_2}(\bar{t}_n)$ obtained via Eq. [21] within a ROI in the middle section of the right lung which comprises 89 pixel and covers an area of 1.39 cm^2 (no. 2 in Table 1). We indeed observe a linear decrease of p_{O_2} with time, thus confirming our assumption a posteriori.

A linear fit to the data yields $p_0 = 0.193(6)$ bar and $R = 0.0039(3)$ bar/s with a χ^2 of 0.91 p.d.f. Consistent with physiology, the initial oxygen concentration is found to be lower in the functional residual capacity (FRC) of the lung than in inspired air. The rate R found for this particular ROI is somewhat higher than the integral expiratory value of 0.002 bar/s mentioned before. However, oxygen uptake is known to vary locally, as well as between different individuals and physiological situations; so the larger value found from our fit seems to us quite possible.

Once the temporal evolution of p_{O_2} is determined, the flip

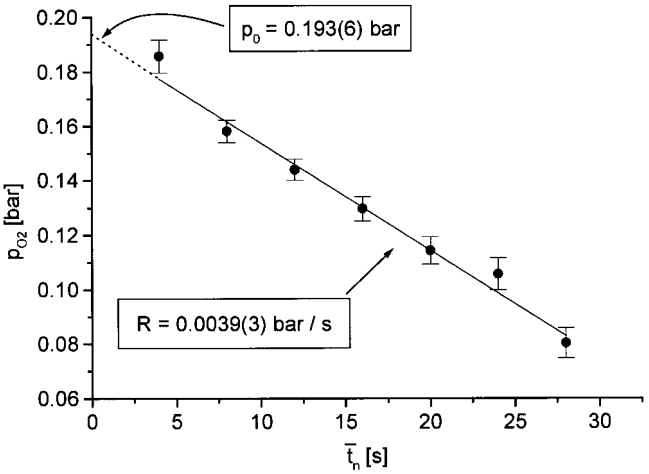

FIG. 5. Temporal development of p_{O_2} in the lung of a living pig. Values of p_0 and R are obtained from linear fitting and extrapolation.

angle α remains the only unknown parameter in Eq. [11]. Considering the uncertainties of intensities as statistical and those of p_0 and R as additional systematic errors, the $\tau = 1$ s series yields $\alpha = 3.36(10)°$ and the $\tau = 7$ s series $\alpha = 3.2(4)°$. Note that the relative error is significantly higher in the latter case, as Γ_{O_2} represents the dominant relaxation mechanism (see Section 5).

4.4. In Vivo Measurement of p_{O_2} in the Human Lung

Images of the lungs of a human volunteer were taken during breathhold after $^3\overrightarrow{He}$ had been administered during spontaneous inspiration of room air. For reasons of comparison with the porcine lung (Section 4.3), a single thick slice (180 mm, coronal orientation) was imaged. Two subsequent series of eight images each with $\tau_1 = 1$ s and $\tau_2 = 5$ s, $U_{RF} = 5$ V were taken. Image analysis was carried out in the same manner as in Section 4.3.

The ROI in the example of Fig. 6 is situated in the upper left lung (no. 4 in Table 1) and comprises 221 pixel (3.45 cm^2). The oxygen partial pressure extracted from the double acquisition is plotted as a function of time. Again, a linear decrease is found. Least squares fitting yields an initial pressure $p_0 = 0.145(5)$ bar and a gradient 0.0017(2) bar/s ($\chi^2 = 0.86$). In comparison to the ROI from the pig lung (Fig. 5), p_0 and R turn out 25 and 58% lower, respectively. The flip angle α as determined from the $\tau = 1$ s series is 1.33(10)°. A calculation based on the $\tau = 5$ s series gives 1.4(5)°, consistent with the first value.

In Table 1 we have compiled p_0 and R values of various ROIs from the porcine lung and the human lung. The positions of the respective ROIs are shown in Fig. 7. For the pig lung, the scatter is about 0.9% for p_0 and 4.5% for R. For the human lung, the respective values are 7.8 and 14.1%.

5. DISCUSSION

The aim of this study was to demonstrate a quantitative determination of time-dependent intrapulmonary oxygen concentrations. The method relies on controlled variation of flip angle or interscan time within one or between two subsequent series of MR images. Analysis is based on the implicit understanding that all other physiological and physical parameters remain unchanged; for instance, it must be assumed that initial oxygen densities and oxygen uptake are the same in both series. If the series are acquired consecutively within one a single sequence, this condition is not fulfilled if $p_{O_2} \neq const;$ hence, two separate imaging series were chosen for the *in vivo* measurements of Sections 4.3 and 4.4. Since image intensities are always normalized to the initial signal, $^3\overrightarrow{He}$ bolus volumes are noncritical in our calculations, as long as the gas composition in the lung is not changed greatly. Due to the good reproducibility of $^3\overrightarrow{He}$ volumes (Section 3.1), variations in oxygen dilution resulting from different bolus volumes lead to a relative error of p_{O_2} of less than 0.5%, which is negligible. (A residual volume of about 850 ml in the pig lung was assumed.) This holds true as long as the total inspiratory volume remains constant, a requirement met automatically if volume controlled ventilation is utilized. Clearly, care must be taken in the case of a freely breathing subject, since large variations in breath volumes lead to substantially different intrapulmonary oxygen concentrations despite equally sized $^3\overrightarrow{He}$ boli. However, in the example of Section 4.4 the volunteer reproduced his mean tidal volume of 850 ml with an accuracy of ± 40 ml. Considering an 80-ml variation of both inspiratory and residual volume (0.85 l and 2 l, respectively), we estimate the contribution to the relative error of p_{O_2} to be about 1.1%.

The double acquisition technique has the obvious disadvantage of not being economical in terms of gas consumption. One might therefore conceive of a single acquisition sequence with a more intricate pattern of nonequal interscan times or with

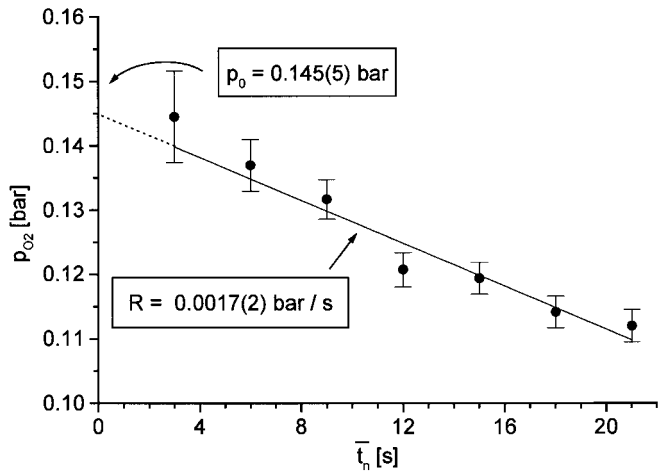

FIG. 6. Temporal development of p_{O_2} in the lung of a human volunteer.

TABLE 1
Results of Initial Oxygen Partial Pressure p_0, Decrease Rate R and Flip Angle α for Different ROIs from a Pig Lung (Volume Controlled Ventilation) and a Human Lung (Spontaneous Breathing)

ROI number	ROI size [pixel]	ROI size [cm^2]	p_0 [bar]	R [bar/s]	α [degrees]	χ^2 [p.d.f.]
Pig						
1	71	1.11	0.188 (6)	0.0039 (3)	3.65 (5)	1.38
2	89	1.39	0.193 (6)	0.0039 (3)	3.36 (10)	0.91
3	57	0.89	0.193 (7)	0.0035 (4)	3.51 (7)	0.99
4	74	1.16	0.192 (7)	0.0039 (4)	3.68 (8)	1.50
Human						
1	129	2.02	0.152 (5)	0.0022 (3)	1.55 (7)	1.14
2	129	2.02	0.156 (6)	0.0025 (3)	1.07 (13)	0.88
3	177	2.77	0.188 (8)	0.0028 (5)	1.11 (20)	1.03
4	221	3.45	0.145 (5)	0.0017 (2)	1.33 (10)	0.86
5	249	3.89	0.148 (4)	0.0021 (2)	1.28 (8)	1.37

Note. ROI positions are shown in Fig. 7. Values for α are calculated from the respective sets of images with $\tau = 1$ s.

combined variation of α and τ and a more complex analysation algorithm. Such investigations are currently under way.

These difficulties nonwithstanding, the accuracy in evaluation of p_{O_2} is remarkable. In the example of the pig (Section 4.3), p_0 and decrease rate R are determined with relative errors of 3 and 7%, respectively. For the first time, this accuracy has been achieved in a local measurement within an area on the order of 1 cm^2.

High signal-to-noise ratios are crucial in these experiments. Hence, signal intensities should be optimized; i.e., one should aim for maximum nuclear polarizations. In future experiments, the use of multislice 2D imaging sequences is conceivable, although an extension of the method to thinner slices will have to consider the loss in SNR due to the decreased number of spins contributing to the image. Preliminary studies have shown, however, that a reduction from a whole lung slice to a 30-mm partition only results in a loss in SNR by a factor of 2 to 3, if a central slice of the lung is chosen. Moreover, if even

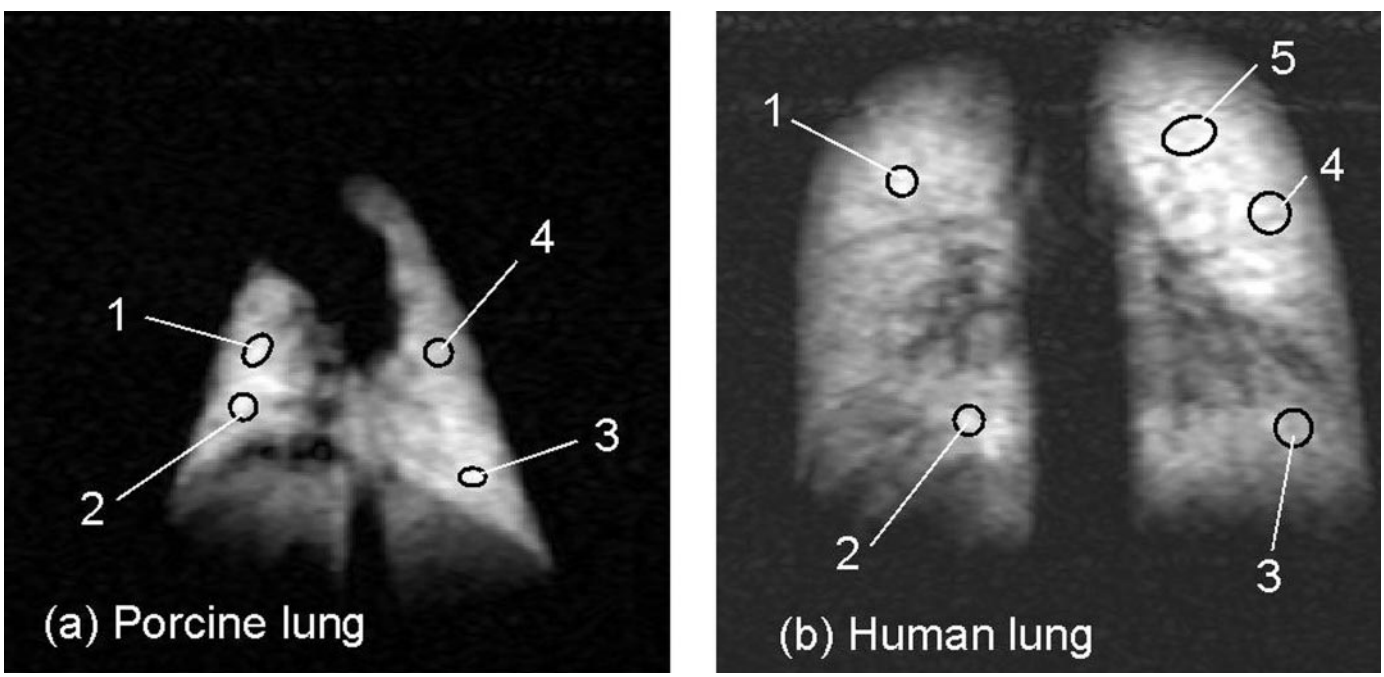

FIG. 7. $^3\overrightarrow{He}$ lung images of (a) a pig and (b) a human volunteer. Exemplary ROIs selected for analysis are shown. Results obtained in these ROIs are listed in Table 1. Field of view is (320 mm)^2.

thinner or more peripheral compartments are imaged, the loss in SNR could generally be compensated for by means of higher flip angles. In the experiment of Section 4.4, flip angles ranged from 1° to 1.5° (see Table 1), so an increase of the RF amplitude by a factor of up to 3 is easily feasible without destroying too much signal. A determination of oxygen concentrations on a scale of $1 \ldots 2$ cm^3 can thus be envisaged.

It ought to be pointed out that the measured decrease rate R is not totally identical with the rate of oxygen uptake by the lung. In the case of a ventilator-maintained inspiratory breathhold, the respirator unit supports a constant pressure in the lung; i.e., volume loss by oxygen uptake is compensated for by automatic supplementation of an equal volume of room air (neglecting the minute release of CO_2 by the lung). In the spontaneously breathing human volunteer, this balance is maintained by air being introduced from anatomical deadspace. In both cases, however, the oxygen concentration in the supplemental air is 21%. The oxygen uptake rate R_u is thus related to R via

$$R = R_u(1 - 0.21), \qquad [22]$$

which means that oxygen uptake in the various ROIs of Table 1 is about 25% greater than the listed values of R.

As for the flip angle, it is in principle possible to compute the value by measuring the voltage that produces a $\pi/2$ pulse on a thermally polarized ^{3}He sample. This calibration method was applied in former experiments of our group [see e.g., (*12*)]. However, there are at least two drawbacks to this: first, flip angles vary when the load of the coil is changed, hence conditions are different for each individual subject. Second, one must account for local magnetic field variations, mainly due to inhomogenieties of the transmit/receive coil. For quantitative applications, one would thus have to calibrate α individually for every subject and various spatial positions. The use of interscan delay variation circumvents this problem, as flip angle depolarization is eliminated mathematically in the determination of p_{O_2}. In a further step, the dataset of either series may then be used to calculate α locally. In all ROIs of the examples in Sections 4.3 and 4.4, flip angles computed from the first series were consistent with those from the second, the set with shorter τ giving more accurate results.

For this study, the centric-reordering sampling scheme, as opposed to a sequentially ordered or variable flip angle (*25*) scheme, was chosen for reasons of mathematical simplicity: The comparison line ($k = 0$) is insensitive to RF depolarization effects in the initial image. This advantage is paid for by slightly deteriorated spatial resolution (as compared to variable flip angle sampling) and contrast (as compared to sequential ordering). However, we believe the differences to be rather small: A recent investigation by Knight-Scott *et al.* (*26*) has shown that both image quality and SNR of constant flip angle and variable flip angle sequences are comparable, the gains in SNR of variable flip angle sequences being likely to be negated by spatial B_1 field inhomogenieties.

Care must be taken that signal intensities, especially of the first images where maximum nuclear polarization is available, stay well within the linear response range of the electronics. Otherwise, the entire algorithm is doomed to failure. Furthermore, for determination of p_{O_2}, values for flip angle α and interscan delay τ should be chosen such as to allow Γ_{O_2} to prevail the relaxation process in one series of images. Recall that $1/\Gamma_{O_2}$ is typically of the order of $10 \ldots 20$ s depending on p_{O_2}. This longitudinal relaxation time has to be compared with the mean depolarization time by RF pulses. By rearranging the expression for $\bar{\Gamma}_{RF}$ (Eq. [8]), we find

$$\bar{T}_{1,RF} = \frac{1}{\bar{\Gamma}_{RF}} = \frac{-\tau}{N \ln(\cos \alpha)} \approx \frac{2\tau}{N\alpha^2}. \qquad [23]$$

The approximation holds for α [radian] $\ll 1$. In the example of Section 4.3, values $\alpha = 56$ mrad ($\triangleq 3.2°$) and $\tau = 7$ s give a mean RF depolarization time $\bar{T}_{1,RF} = 55$ s, which is distinctly larger than T_{1,O_2}. Moreover, if R is measured via variation of τ, the accuracy depends on the difference $\Delta\tau = \tau_2 - \tau_1$. Considering that R is determined from the slope of a linear fit (Eq. [20]), the error ΔR of which is calculated by means of the matrix of covariance, it is straightforward to show that ΔR scales proportional to $(\Delta\tau^2 + 2\tau_1\Delta\tau)^{-1}$. So ΔR is minimized for large $\Delta\tau$. This justifies the choice of parameters for the determination of time-dependent p_{O_2} in Sections 4.3 and 4.4.

6. CONCLUSION AND PERSPECTIVES

The *in vivo* effect of O_2 upon the longitudinal relaxation time T_1 offers an instrument for analysis of intrapulmonary oxygen concentrations. Appropriate selection of operator accessible parameters of image acquisition allows one to determine regional p_{O_2}, its time course, and regional flip angles. The accuracy of the presented method is, overall, at least equivalent to conventional methods of oxygen analysis in respiratory gases. The superiority of this novel approach lies both in its ability to provide high regional resolution, and in its noninvasiveness. Since intrapulmonary distribution of p_{O_2} is governed by both regional ventilation, regional perfusion, and oxygen uptake, the method constitutes a new approach to lung function analysis. We know that in lung diseases, the distribution of oxygen is often not homogenous due to disturbances of ventilation, perfusion, or mismatch of both. The final assessment of the method as well as a proper evaluation of its medical potential requires, of course, an extension of these measurements to a larger sample of healthy volunteers as well as patients with lung disease. This task can only be fulfilled by means of an automatic computer controlled analysis of regional oxygen concentration and uptake. The mathematical foundation has been provided in this paper and its implementation into

the postprocessing software is in preparation. This will allow online acquisition and processing of data, and instantaneous availability of diagnostic information to the physician.

ACKNOWLEDGMENTS

We acknowledge funding by the Deutsche Forschungsgemeinschaft DFG, Grant TH315/8-1, by the Innovationsstiftung des Landes Rheinland-Pfalz and by the Institut für Diagnostikforschung (IDF), and we thank J. Bermuth for many helpful discussions.

REFERENCES

1. H. Middleton, R. D. Black, B. Saam, G. D. Cates, G. P. Cofer, R. Guenther, W. Happer, L. W. Hedlund, G. A. Johnson, K. Juvan, and J. Swartz, MR imaging with hyperpolarized ^{3}He gas, *Magn. Res. Med.* **33,** 271–275 (1995).
2. P. Bachert, L. R. Schad, M. Bock, M. V. Knopp, M. Ebert, T. Großmann, W. Heil, D. Hofmann, R. Surkau, and E. W. Otten, Nuclear magnetic resonance imaging of airways in humans with use of hyperpolarized ^{3}He, *Magn. Res. Med.* **36,** 192–196 (1996).
3. M. Ebert, T. Großmann, W. Heil, E. W. Otten, R. Surkau, M. Leduc, P. Bachert, M. V. Knopp, L. R. Schad, and M. Thelen, Nuclear magnetic resonance imaging with hyperpolarized ^{3}He, *Lancet* **347,** 1297–1299 (1996).
4. J. R. MacFall, H. C. Charles, R. D. Black, H. Middleton, J. C. Swartz, B. Saam, B. Driehuys, C. Erickson, W. Happer, G. D. Cates, G. A. Johnson, and C. E. Ravin, Human lung air spaces: Potential for MR imaging with hyperpolarized ^{3}He, *Radiology* **200,** 553–558 (1996).
5. R. D. Black, H. L. Middleton, G. D. Cates, G. P. Cofer, B. Driehuys, W. Happer, L. W. Hedlund, G. A. Johnson, M. D. Shattuck, and J. C. Swartz, In vivo He-3 MR images of guinea pig lungs, *Radiology* **199,** 867–870 (1996).
6. G. A. Johnson, G. Cates, X. J. Chen, G. P. Cofer, B. Driehuys, W. Happer, L. W. Hedlund, B. Saam, M. D. Shattuck, and J. Swartz, Dynamics of magnetization in hyperpolarized gas MRI in the lung, *Magn. Res. Med.* **38,** 66–71 (1997).
7. L. Darrasse, G. Guillot, P. J. Nacher, and G. Tastevin, Low-field ^{3}He nuclear magnetic resonance in human lungs, *C. R. Acad. Sci.* **324,** 691–700 (1997).
8. M. S. Albert, G. D. Cates, B. Driehuys, W. Happer, B. Saam, C. S. Springer Jr., and A. Wishnia, Biological magnetic resonance imaging using laser-polarized ^{129}Xe, *Nature* **137,** 199–201 (1994).
9. M. E. Wagshul, T. M. Button, H. F. Li, Z. Liang, C. S. Springer, K. Zhong, and A. Wishnia, In vivo MR imaging and spectroscopy using hyperpolarized ^{129}Xe, *Magn. Res. Med.* **36,** 183–191 (1996).
10. K. Sakai, A. M. Bilek, E. Oteiza, R. L. Walsworth, D. Balamore, F. A. Jolesz, and M. Albert, Temporal dynamics of hyperpolarized ^{129}Xe resonances in living rats, *J. Magn. Reson. B* **111,** 300–304 (1996).
11. J. P. Mugler, B. Driehuys, J. R. Brookeman, G. D. Cates, S. S. Berr, R. G. Bryant, T. M. Daniel, E. E. de Lange, J. H. Downs Jr., C. J. Erickson, W. Happer, D. P. Hinton, N. F. Kassel, T. Maier, C. D. Phillips, B. T. Saam, K. L. Sauer, and M. E. Wagshul, MR imaging and spectroscopy using hyperpolarized ^{129}Xe gas: Preliminary human results, *Magn. Res. Med.* **37,** 809–815 (1997).
12. H.-U. Kauczor, D. Hofmann, K.-F. Kreitner, H. Nilgens, R. Surkau, W. Heil, A. Pottast, M. Knopp, E. W. Otten, and M. Thelen, Normal and abnormal pulmonary ventilation: Visualization at hyperpolarized He-3 MR imaging, *Radiology* **201,** 564–568 (1996).
13. H.-U. Kauczor, M. Ebert, K.-F. Kreitner, H. Nilgens, R. Surkau, W. Heil, D. Hofmann, E. W. Otten, and M. Thelen, Imaging of the lungs using 3He MRI: Preliminary clinical experience in 18 patients with and without lung disease, *J. Magn. Reson. Imag.* **7,** 538–543 (1997).
14. B. Saam, W. Happer, and H. Middleton, Nuclear relaxation of ^{3}He in the presence of O_2, *Phys. Rev. A* **52,** 862–865 (1995).
15. B. Eberle, N. Weiler, K. Markstaller, H.-U. Kauczor, A. Deninger, M. Ebert, T. Grossmann, W. Heil, L. O. Lauer, T. P. L. Roberts, W. G. Schreiber, R. Surkau, W. F. Dick, E. W. Otten, and M. Thelen, Analysis of intrapulmonary O_2-concentrations by magnetic resonance imaging of inhaled hyperpolarized ^{3}Helium, *J. Appl. Physiology,* in press.
16. N. R. Newbury, A. S. Barton, G. D. Cates, W. Happer, and H. Middleton, Gaseous ^{3}He–^{3}He magnetic dipolar spin relaxation, *Phys. Rev. A* **48**(6), 4411–4420 (1993).
17. L. D. Schearer and G. K. Walters, Nuclear spin-lattice relaxation in the presence of magnetic-field gradients, *Phys. Rev.* **139**(5A), 1398–1402 (1965).
18. G. D. Cates, S. R. Schaefer, and W. Happer, Relaxation of spins due to field inhomogeneities in gaseous samples at low magnetic fields and low pressures, *Phys. Rev. A* **37,** 2877–2885 (1988).
19. G. Eckert, W. Heil, M. Meyerhoff, E. W. Otten, R. Surkau, M. Werner, M. Leduc, P. J. Nacher, and L. D. Schearer, A dense polarized ^{3}He target based on compression of optically pumped gas, *Nucl. Instrum. Methods A* **320,** 53–65 (1992).
20. J. Becker, W. Heil, B. Krug, M. Leduc, M. Meyerhoff, P. J. Nacher, E. W. Otten, Th. Prokscha, L. D. Schearer, and R. Surkau, Study of mechanical compression of spin-polarized ^{3}He gas, *Nucl. Instrum. Methods A* **346,** 45–51 (1994).
21. W. Heil, H. Humblot, E. W. Otten, M. Schäfer, R. Surkau, and M. Leduc, Very long nuclear relaxation times of spin polarized helium 3 in metal coated cells, *Phys. Lett. A* **201,** 337–343 (1995).
22. R. Surkau, J. Becker, M. Ebert, T. Großmann, W. Heil, D. Hofmann, H. Humblot, M. Leduc, E. W. Otten, D. Rohe, K. Siemensmeyer, M. Steiner, F. Tasset, and N. Trautmann, Realization of a broad band neutron spin filter with compressed, polarized ^{3}He gas, *Nucl. Instrum. Methods A* **384,** 444–450 (1997).
23. R. M. Henkelman, Measurement of signal intensities in the presence of noise in MR images, *Med. Phys.* **12,** 232–233 (1985). [Erratum: *Med. Phys.* **13,** 544 (1986)]
24. H. Gudbjartsson and S. Patz, The Rician distribution of noisy MRI data, *Magn. Res. Med.* **34,** 910–914 (1995).
25. L. Zhao, R. Mulkern, C. H. Tseng, D. Williamson, S. Patz, R. Kraft, R. Walsworth, F. Jolesz, and M. Albert, Gradient-echo imaging considerations for hyperpolarized ^{129}Xe MR, *J. Magn. Reson. B* **113,** 179–183 (1996).
26. J. Knight-Scott, V. M. Mai, J. P. Mugler III, J. R. Brookeman, Considerations in using the variable-flip-angle method in laser polarized magnetic resonance gas imaging and spectroscopy experiments, *Proc. Intl. Soc. Magn. Res. Med.* **7,** 2092 (1999).